Geophysical Journal International

Geophys. J. Int. (2015) **202,** 1088–1095 doi: 10.1093/gji/ggv192
GJI Marine geosciences and applied geophysics

Water saturation effects on *P*-wave anisotropy in synthetic sandstone with aligned fractures

Kelvin Amalokwu,[1,2] Mark Chapman,[3,4] Angus I. Best,[1] Timothy A. Minshull[2] and Xiang-Yang Li[4]

[1]*National Oceanography Centre, Southampton University of Southampton, Waterfront Campus, European Way, Southampton SO*14 3*ZH, United Kingdom. E-mail: kelvin.amalokwu@noc.soton.ac.uk*
[2]*University of Southampton, National Oceanography Centre, Southampton European Way, Southampton SO*14 3*ZH, United Kingdom*
[3]*University of Edinburgh School of Geosciences, Grant Institute, the King's Building, West Mains Road, Edinburgh EH*9 3*JW, United Kingdom*
[4]*Edinburgh Anisotropy Project, British Geological Survey, Murchison House, West Mains Road, Edinburgh EH*9 3*LA, United Kingdom*

Accepted 2015 May 1. Received 2015 April 30; in original form 2015 March 12

SUMMARY

The seismic properties of rocks are known to be sensitive to partial liquid or gas saturation, and to aligned fractures. *P*-wave anisotropy is widely used for fracture characterization and is known to be sensitive to the saturating fluid. However, studies combining the effect of multiphase saturation and aligned fractures are limited even though such conditions are common in the subsurface. An understanding of the effects of partial liquid or gas saturation on *P*-wave anisotropy could help improve seismic characterization of fractured, gas bearing reservoirs. Using octagonal-shaped synthetic sandstone samples, one containing aligned penny-shaped fractures and the other without fractures, we examined the influence of water saturation on *P*-wave anisotropy in fractured rocks. In the fractured rock, the saturation related stiffening effect at higher water saturation values is larger in the direction across the fractures than along the fractures. Consequently, the anisotropy parameter 'ε' decreases as a result of this fluid stiffening effect. These effects are frequency dependent as a result of wave-induced fluid flow mechanisms. Our observations can be explained by combining a frequency-dependent fractured rock model and a frequency-dependent partial saturation model.

Key words: Fracture and flow; Body waves; Seismic anisotropy; Acoustic properties.

1 INTRODUCTION

Experimental and theoretical studies have long shown that seismic waves are strongly affected by the presence of partial gas saturation and by the presence of aligned fractures, the latter causing seismic anisotropy. Shear waves are considered to be more reliable indicators of fracture properties (e.g. fracture orientation and density) than *P* waves. However, the use of *P* waves for fracture characterization has received considerable attention since *P* waves form the basis of most commercial seismic surveys (Sayers & Rickett 1997). Consequently *P*-wave anisotropy has been extensively studied and is widely used for fracture characterization (e.g. Winterstein 1986; Lynn *et al.* 1996; Rüger 1997; Li 1999). *P* waves have the potential not only to characterize fractures but also of discriminating between saturating fluids (Rüger & Tsvankin 1997; Bakulin *et al.* 2000). Liquid (brine, oil) and gas usually share the available pore space in reservoirs containing gas (Gregory 1976), making it necessary to understand the combined effects of multiphase saturation and fractures on seismic wave propagation for improved reservoir characterization. However, multiphase saturation effects on seismic anisotropy of fractured rock are still poorly understood even though such conditions are common. Such know-how would be useful for characterization of fractured hydrocarbon reservoirs containing gas and geothermal steam reservoirs. Important applications could also be found in seismic time-lapse monitoring of gas injection into hydrocarbon reservoirs for enhanced oil recovery; and for the geologic storage of carbon dioxide (CO_2) where fractures can serve as leakage pathways (Carcione *et al.* 2013).

P-wave velocity anisotropy in fractured rocks is known to depend on saturating fluid and is frequency-dependent due to wave-induced fluid flow (Chapman *et al.* 2003; Gurevich *et al.* 2009; Tillotson *et al.* 2014). The presence of partial gas saturation is also known to affect *P*-wave velocities in a frequency-dependent way (White 1975; Murphy 1984; Cadoret *et al.* 1995; Carcione *et al.* 2003). Fracture and fluid properties are inferred from seismic data using theoretical models. As such, there is a desire to validate theoretical models using controlled experiments. Experimental studies of partial liquid/gas saturation effects on *P*-wave velocities have been presented for isotropic rocks (Murphy 1984; Bourbie & Zinszner 1985; Cadoret *et al.* 1995; King *et al.* 2000), however, the

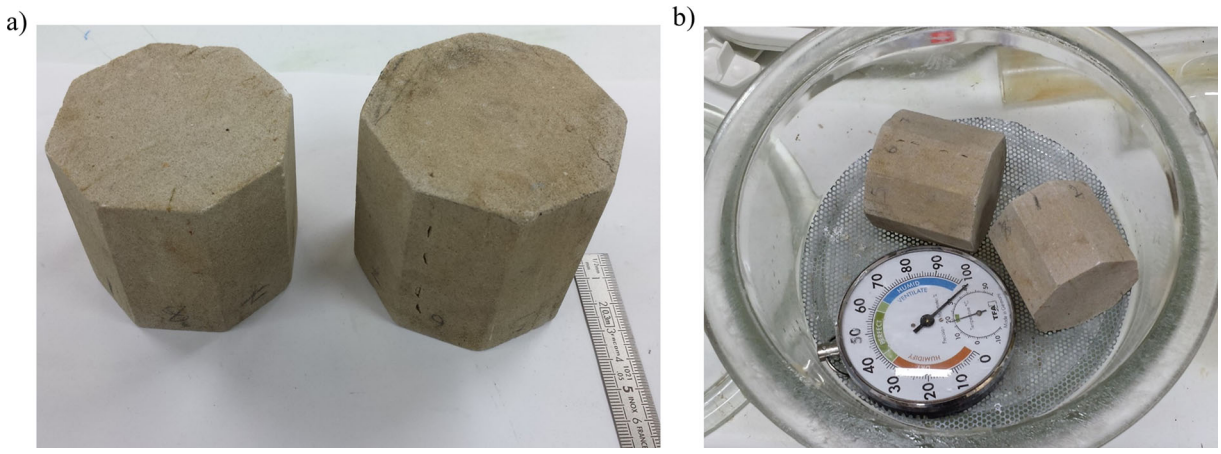

Figure 1. (a) Rock samples used in this study (blank sample on the left and fractured sample on the right), (b) relative humidity method used to achieve partial saturation.

effect of partial liquid/gas saturation on *P*-wave velocity (and hence *P*-wave anisotropy) in fractured rocks remains unknown. Also, a handful of controlled fractured rock experiments have been carried out (e.g. Rathore *et al.* 1995; Tillotson *et al.* 2011; Tillotson *et al.* 2014) and results have been compared to theoretical models such as the models of Hudson (1981), Thomsen (1995) and Chapman *et al.* (2003). However, theoretical and experimental studies of fluid effects on *P*-wave anisotropy have focused primarily on single fluid phases (100 per cent gas or liquid saturation). To date, no experimental study has been carried out to observe the effects of water saturation on *P*-wave anisotropy in fractured rocks.

This work examines the influence of two-phase (liquid-gas) saturations (which would be referred to here as partial saturation) on *P*-wave anisotropy in fractured rocks. Using an octagonal-shaped synthetic sandstone sample containing aligned penny-shaped fractures, we present laboratory measurements of water saturation effects on *P*-wave anisotropy. These novel results show an interesting sensitivity of *P*-wave anisotropy to changing water saturation. Qualitative agreement with theory was found by combining the corrected White (1975) model for partial saturation (sometimes referred to as the White and Dutta-Ode model—see Mavko *et al.* 2009) with the fractured rock model of Chapman (2003) using similar ideas presented by Amalokwu *et al.* (2015). As pointed out by Tillotson *et al.* (2014), the ultrasonic wavelengths used were close to the size (diameter) of the penny-shaped voids (fractures), in common with previously reported experimental results of this nature. Nevertheless, Tillotson *et al.* (2014) found several useful correlations between the data and the model of Chapman (2003), which suggest that the model predictions are reasonably unaffected by scattering (Tillotson *et al.* 2014). Our experiments appear also to be little affected by scattering because we were able to explain saturation effects using equivalent medium modelling.

2 METHODS

2.1 Synthetic rock samples

A detailed description of the synthetic rock samples used in this study can be found in the paper by Tillotson *et al.* (2014). Two octagonal samples (Fig. 1) were used in this study—one fractured sample and a blank sample (rock sample without fractures). The rock samples were made from a mixture of sand, kaolinite and aqueous sodium silicate gel and then the mixture was packed into a mould in successive layers. A predetermined number aluminium discs were distributed on top of each layer of sand mixture for the creation of penny-shaped voids. After the sandstone was formed by heating and drying, the aluminium discs were leached out using hydrochloric acid, leaving blank penny-shaped voids. Image analysis of X-ray CT scans was used to obtain the fracture density, $\varepsilon_f = 0.0314 \pm 0.0059$, mean fracture radius of 2.91 ± 0.06 mm, and mean fracture aspect ratio of 0.0429 ± 0.0008. Porosity is 30 and 33 per cent for the blank and fractured sample, respectively, and permeability for both samples is 21 mD (see Tillotson *et al.* 2014). As pointed out by Tillotson *et al.* (2014), the advantage of these octagonal samples is that we can measure the full elastic wave tensor on single sandstone samples and thus gain an unambiguous dataset for comparison with theoretical models.

2.2 Ultrasonic measurements

We measured ultrasonic *P*-wave velocity using a laboratory benchtop pulse transmission system with one inch-diameter broad-band ultrasonic transducers with a central frequency of 500 kHz placed on each of four sets of opposing sides of the octagonal samples, thus allowing measurement of velocity at different angles. A more detailed description of the technique is given by Tillotson *et al.* (2014). To ensure consistent coupling between experiments, a pneumatic ram applied a pressure of 60 psi to the transducer faces in contact with the samples, and couplant was carefully reapplied to the transducer faces between experiments. *P*-wave velocity was measured for wave propagation at 0°, 45° and 90° to the fracture/bedding normal.

Velocity was calculated by comparing the broad-band signals from the rock samples with those of a duralumin reference sample (with known elastic properties). Velocity was calculated by comparing the Fourier phase angle spectra of the rock and reference wavelets using

$$V_1(f) = \frac{x_1}{\Delta t(f) + \frac{x_2}{V_2}}, \tag{1}$$

where $V_1(f)$ is the velocity of the rock sample, x_1 is the wave propagation distance in the rock sample, $\Delta t(f)$ is the difference in traveltime calculated from the Fourier phase angle spectra of the rock $\varphi_{\text{sample}}(f)$ and reference $\varphi_{\text{reference}}(f)$ sample according to $\Delta t = t_{\text{sample}} - t_{\text{reference}} = \frac{[\varphi_{\text{sample}}(f) - \varphi_{\text{reference}}(f)]}{2\pi f}$, x_2 is the wave

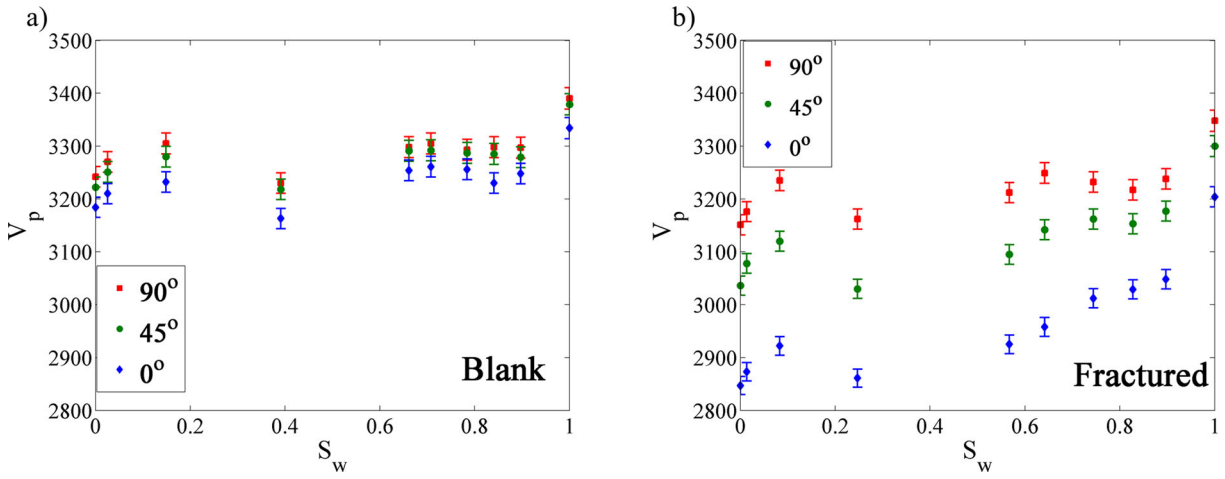

Figure 2. *P*-wave modulus versus S_w at 0° (blue diamond), 45° (green circle) and 90° (red square) for the (a) blank sample (b) fractured sample. Vertical error bars show error estimates.

propagation distance in the reference sample, and V_2 is the velocity of duralumin (taken to be 6398 m s^{-1} for *P* waves for all frequencies as duralumin is non-dispersive). The velocity measurements were corrected for frequency-dependent diffraction effects as a result of beam spreading from the transducer face (Best 1992). We used isotropic diffraction corrections only.

Ultrasonic wave measurements were then taken at different partial saturation states of air/water (see the Supporting Information for details of saturation methods used), quantified by water saturation S_w. Velocity was measured to an accuracy of ±0.6 per cent and results are presented at a single frequency of 500 kHz (see Tillotson *et al.* 2014).

The numerical modelling experiment of wave propagation in anisotropic media by Dellinger & Vernik (1994) showed that if the wave front is propagating parallel or perpendicular to the layering (or in this case fractures), a true phase velocity is measured in laboratory ultrasonic experiments. However, for wave propagation at 45° to the fracture normal, the wave front can suffer a lateral displacement dependent on the length of the sample and the strength of the anisotropy. If the lateral translation suffered by the wave is greater than the radius of the receiving transducer, then a group velocity is measured, not a phase velocity. Using eq. (1) from Dellinger & Vernik (1994) to calculate the lateral translations, we get a value of 2.9 mm for the *P* wave. We can conclude we measure phase velocity in our experimental setup as our transducer radius of 12.7 mm is much larger than the lateral translations suffered by the wave fronts. A similar conclusion was reached by Tillotson *et al.* (2014) using the same experimental setup as that used in this study.

3 RESULTS

The blank rock velocity results (Fig. 2a) show minimal velocity anisotropy due to layering from the manufacturing process. *P*-wave velocity is at a maximum at 90° and a minimum at 0° to the bedding/layer normal. The velocity versus S_w trend is similar in the three directions. The general trend for each propagation direction is an increase in *P*-wave velocity with increasing S_w apart from a decrease at $S_w \approx 0.40$, the highest velocity occurring at $S_w = 1.0$. These results are in agreement with published ultrasonic data (e.g. Gregory 1976; Murphy 1984; Bourbie & Zinszner 1985).

Fig. 2(b) shows *P*-wave velocity versus S_w relationship at 0°, 45° and 90° to the fracture normal. Here we see significant angular variation in velocity as expected. Similar to the blank sample, the velocity versus S_w trend is similar in all three directions and is similar to that observed in the blank rock. The data trend suggests evidence of frequency dispersion (attributed to wave-induced fluid flow), which can be seen in the data from the steady increase in velocity from dry to full water saturation in contrast to Gassmann's low frequency predictions (see Murphy 1982; Mavko & Nolen-Hoeksema 1994). There is considerable literature on saturation related dispersion resulting from wave induced fluid flow (see Müller *et al.* 2010). In this paper we will focus mainly on the differences between the blank and the fractured sample response to changing water saturation.

In order to remove any ambiguity caused by the effect of fluid saturation on bulk density, we calculated the *P*-wave moduli, $M = \rho V^2$, (Fig. 3) in all three directions (equivalent to stiffness components C_{11} and C_{33} for the 90° and 0° directions, respectively). In the blank sample (Fig. 3a), all three directions show similar *M* versus S_w trends, with *M* increasing from $S_w = 0$ to $S_w \approx 0.15$, staying fairly constant between $S_w \approx 0.15$ and $S_w \approx 0.40$, after which there is a steady increase until $S_w = 1.0$. The fractured sample (Fig. 3b) shows a similar trend to that observed in the blank sample, with *M* increasing from $S_w = 0$ to $S_w \approx 0.10$, staying fairly constant between $S_w \approx 0.10$ and $S_w \approx 0.25$, after which there is a steady increase until $S_w = 1.0$.

Fig. 4 shows plots of Thomsen-style *P*-wave anisotropy parameter (see Thomsen 1986), 'epsilon' (ε) versus S_w. The parameter (ε) represents the difference in *P*-wave velocity between the vertical (90°) and horizontal (0°) directions and is given by $\varepsilon = \frac{c_{11}-c_{33}}{2c_{33}}$. The blank sample shows a fairly constant value of ε (Fig. 4a) while a decrease in ε can be seen in the fractured sample at higher values of S_w (Fig. 4b).

Fig. 5 shows plots of the *P*-wave moduli from Fig. 3 at the different S_w values normalized by their individual dry values ($S_w = 0$). The data points almost overlap in the blank sample (Fig. 5a), however, in the fractured sample the fluid effect appears to be maximum at 0°, intermediate at 45° and minimum at 90° to the fracture normal at higher S_w values (~0.75–1.0; Fig. 5b).

4 MODELLING INSIGHT AND DISCUSSIONS

Analysis here will focus on the effect of water saturation on the *P*-wave moduli (anisotropic) and on the *P*-wave anisotropy

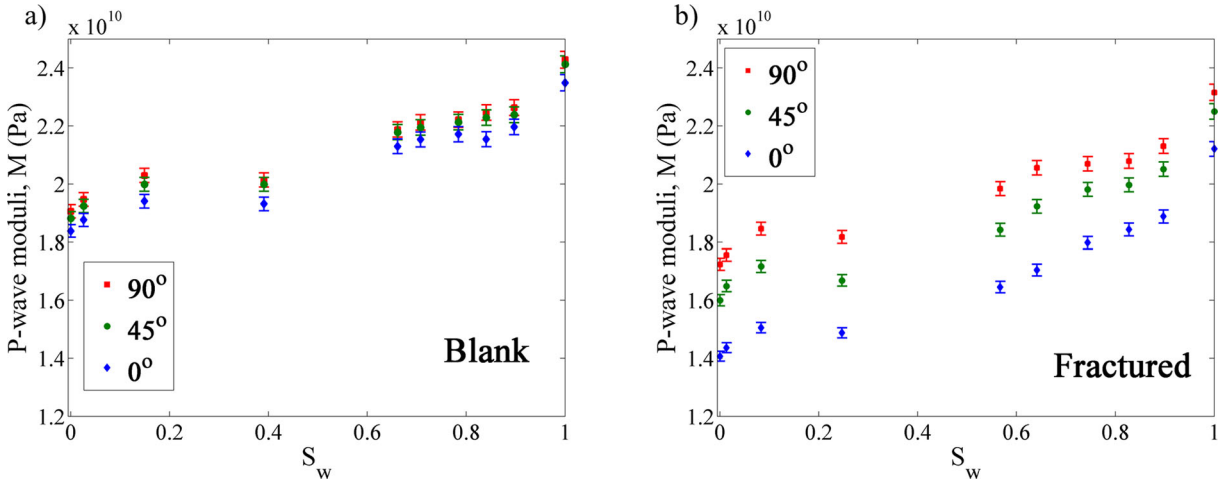

Figure 3. *P*-wave modulus versus S_w at 0°, 45° and 90° for the (a) blank sample and (b) fractured sample. Vertical error bars show error estimates.

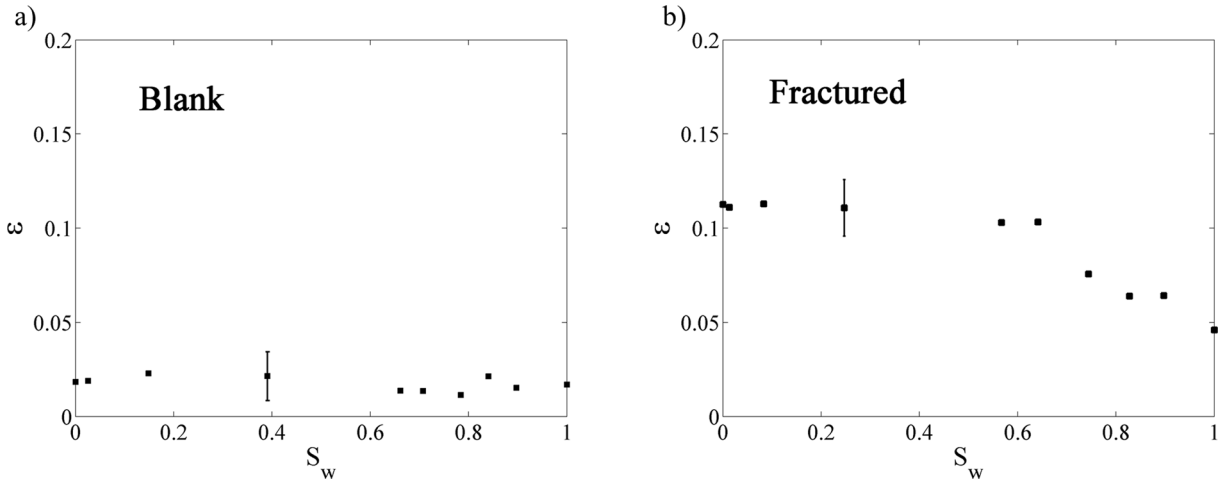

Figure 4. Measured *P*-wave anisotropy parameter (ε) versus S_w for the (a) blank sample and (b) for the fractured sample. Vertical error bars show error estimates.

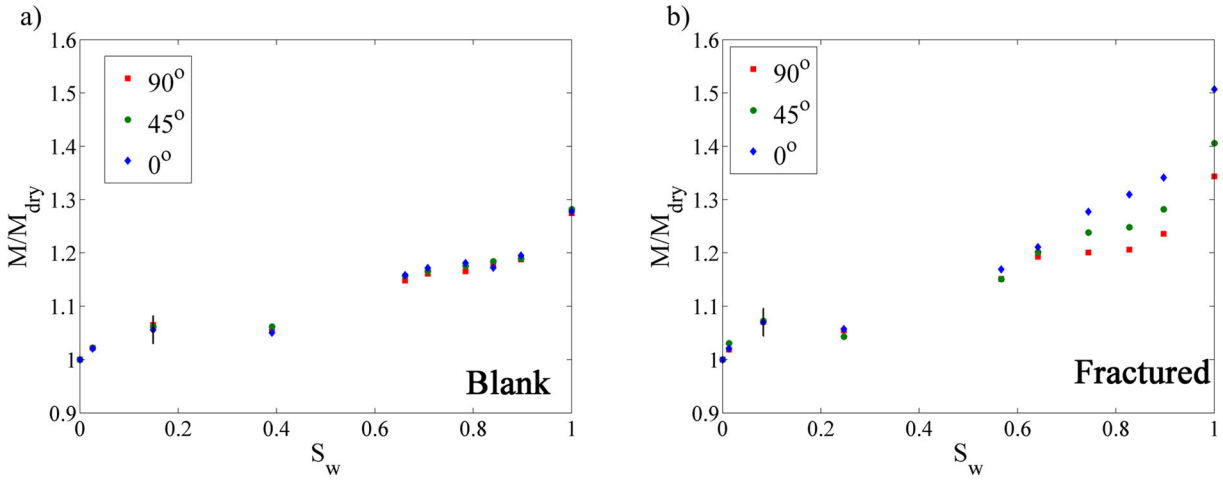

Figure 5. Ratios of the *P*-wave modulus to the dry *P*-wave modulus versus S_w at 0°, 45° and 90° for the (a) blank rock and (b) for the fractured rock. Vertical error bars show error estimates.

parameter, ε. There is a lack of suitable frequency-dependent theoretical models for elastic wave velocities in partially saturated fractured rocks. Using the same method as Amalokwu *et al.* (2015) we combine two models to give some insight into the possible mechanisms in our experiments. We combine the fractured rock model of Chapman (2003) and the partial saturation model of White (1975). The stiffness tensor, C_{ijkl}, given by Chapman (2003) relating the contributions from the isotropic elastic tensor (C^0, with Lamé

parameters, λ and μ), C^1 (pores), C^2 (microcracks) and C^3 (fractures) scaled by the porosity (Φ_p), microcrack density (ε_c) and fracture density (ε_f) is of the form:

$$C_{ijkl} = C^0_{ijkl} - \Phi_p C^1_{ijkl} - \varepsilon_c C^2_{ijkl} - \varepsilon_f C^3_{ijkl} \quad (2)$$

This model is not designed for partial saturation, so in the elastic tensors, we replace all terms apart from the fracture correction, with the Lamé parameters λ° and μ° obtained from the model of White (1975) for each water saturation value. The Lamé parameters λ° and μ° from White's model already contain porosity effects, and as shown by Chapman *et al.* (2003), ε_c can be set to zero in high porosity rocks which would make the contribution from C^2 zero. We now have an equation of the form:

$$C_{ijkl} = C^{iso}_{ijkl}(\lambda^o, \mu^o) - \varepsilon_f C^3_{ijkl}; \quad (3)$$

where the term C^{iso}_{ijkl} is obtained from the Lamé parameters λ° and μ° calculated using the model of White (1975) (see Mavko *et al.* 2009, p. 327), after which the fracture correction C^3 from the model of Chapman *et al.* (2003) is applied. It should be pointed out here that the Lamé parameter, μ° is the rock shear modulus which is assumed to be unaffected by saturation in White's model. In our modelling approach, the dispersion as a result of partial saturation is obtained from the model of White (1975) while anisotropy and dispersion from the fractures are obtained from the model of Chapman (2003). We do not seek to model directly our experimental results but rather propose an explanation for our observations using a simple modelling exercise. We point out that dispersion as a result of partial saturation had to be included since the fractured rock model of Chapman (2003) was not developed for multiphase saturations. White's model was used to model this dispersion because it is a simple frequency-dependent saturation model; however, the cause of the dispersion in the partially saturated case is not restricted to patchy saturation. The idea here is to achieve frequency-dependent bulk moduli caused by stiffening of the frame due to the presence of partial saturation. White's model could be replaced with any other model that incorporates a frequency-dependent stiffening mechanism (e.g. viscous squirt flow).

Model predictions were calculated using the same blank rock properties as those used by Amalokwu *et al.* (2015) as input into White's model and a fracture density, $\varepsilon_f = 0.0314$ for the model of Chapman *et al.* (2003). The gas patch radius in White's model was kept constant (0.5 mm) and the frequency was varied, however, similar plots can be reproduced by varying the gas patch size and keeping the frequency constant. The model of Chapman (2003) was developed for single-phase saturation, therefore, in order to adapt this model for multiphase saturation, we require an effective fluid bulk modulus as input for the fluid bulk modulus in the model of Chapman (2003). Taking the effective fluid modulus as the Reuss average (see Mavko *et al.* 2009) of air and water bulk moduli, no additional dispersion is obtained at partial saturation from the fractured rock model as shown by Amalokwu *et al.* (2015). The Reuss average corresponds to the low frequency case where the gas and liquid are mixed uniformly, so the wave-induced pore pressures have enough time to equilibrate during a seismic period (Mavko & Mukerji 1998). The Reuss average of the bulk moduli of air and water gives an effective fluid bulk modulus which is equivalent to the bulk modulus of air from full air (gas) saturation to very close to full water saturation (~2 per cent air saturation). Consequently, the fractured model does not show any dispersion at partial saturation and this might not be the case at higher frequencies.

The Reuss average is known to underpredict the effective fluid moduli when the wave-induced pore pressures do not have enough time to equilibrate during a seismic period and in this case other mixing laws (see Mavko *et al.* 2009) should be used to calculate the effective fluid moduli. However, instead of using fluid mixing laws (e.g. Brie *et al.* 1995) or explicitly calculating the dynamic fluid modulus (e.g. Yao *et al.* 2013; which could achieve similar effects we are attempting to show), we will take an effective fluid modulus equivalent to the fluid stiffening effect from White's model (compared to Gassmann's low-frequency predictions). We do this by taking the real part of the frequency-dependent bulk modulus obtained from White's model as the saturated rock bulk modulus and then by re-arranging Gassmann's equation, we can obtain the fluid bulk modulus. We then take this fluid bulk modulus as the bulk modulus for input into the fractured rock model. Our purpose here is to illustrate the potential effect of additional dispersion at partial saturation from the fractured rock model, which we require to achieve a better agreement with our experimental results. However, we can only obtain this additional dispersion by assuming an effective fluid modulus which is not the Reuss average of air and water, suggesting we need to consider the case where the fluid mixture within the cracks is not the Reuss average of air and water (hence unrelaxed) as this could play an important role in the effective stiffness of the fractures. This effective fluid modulus would be frequency-dependent, similar to the case in isotropic rocks. Using the approach we have adopted, the fluid bulk modulus effect would be consistent in both the background isotropic rock model and the fractured rock model at each frequency (although this might not be the case in reality). We take the microcrack relaxation timescale (see Chapman 2003; Chapman *et al.* 2003) to be the same ($\tau_m = 2.4 \times 10^{-8}$ s) as that used for the same rock sample by Tillotson *et al.* (2014).

Fig. 6(a) shows the frequency-dependent bulk modulus obtained from the model of White (1975) and Fig. 6(b) shows the corresponding effective fluid moduli which is used as an input into the fractured rock model. A fracture correction using the model of Chapman (2003) was then applied and 'ε' calculated for all frequencies corresponding to those used in White's model (Fig. 6c). Initially, we consider dispersion solely from White's model. As a result of White's model being consistent with Gassmann's predictions at full water saturation because no patches exist at full water saturation, no dispersion occurs at full water saturation ('ε' is the same at all frequencies). To include dispersion from the fractured model, we set the frequency in the model of Chapman (2003) equal to that used in White's model. It can be seen that 'ε' becomes frequency dependent both at partial saturation (higher S_w values) and full water saturation, with 'ε' decreasing as frequency increases. In order to compare the observed experimental trend to our modelling results (Fig. 6d), we used a fracture density of 0.034 (within the uncertainty range for the fracture density, $\varepsilon_f = 0.0314 \pm 0.0059$) in order to fit the dry value for 'ε', leaving other parameters the same as given above. We see better agreement with the trend when additional dispersion from the fractured rock model is considered.

Using the same results from the modelling above, we calculated the anisotropic *P*-wave moduli. We plot the *P*-wave anisotropic moduli at 500 kHz with dispersion from White's model alone (Fig. 7a) and then with additional dispersion from the fractured rock model of Chapman (2003) (Fig. 7b). We see that when dispersion from the fractured model is considered, the fluid effect at higher S_w values is greater in both the 0° and 45° directions, with a more pronounced effect at 0°. This is more obvious when the *P*-wave moduli are normalized with their dry values ($S_w = 0$; Figs 7c

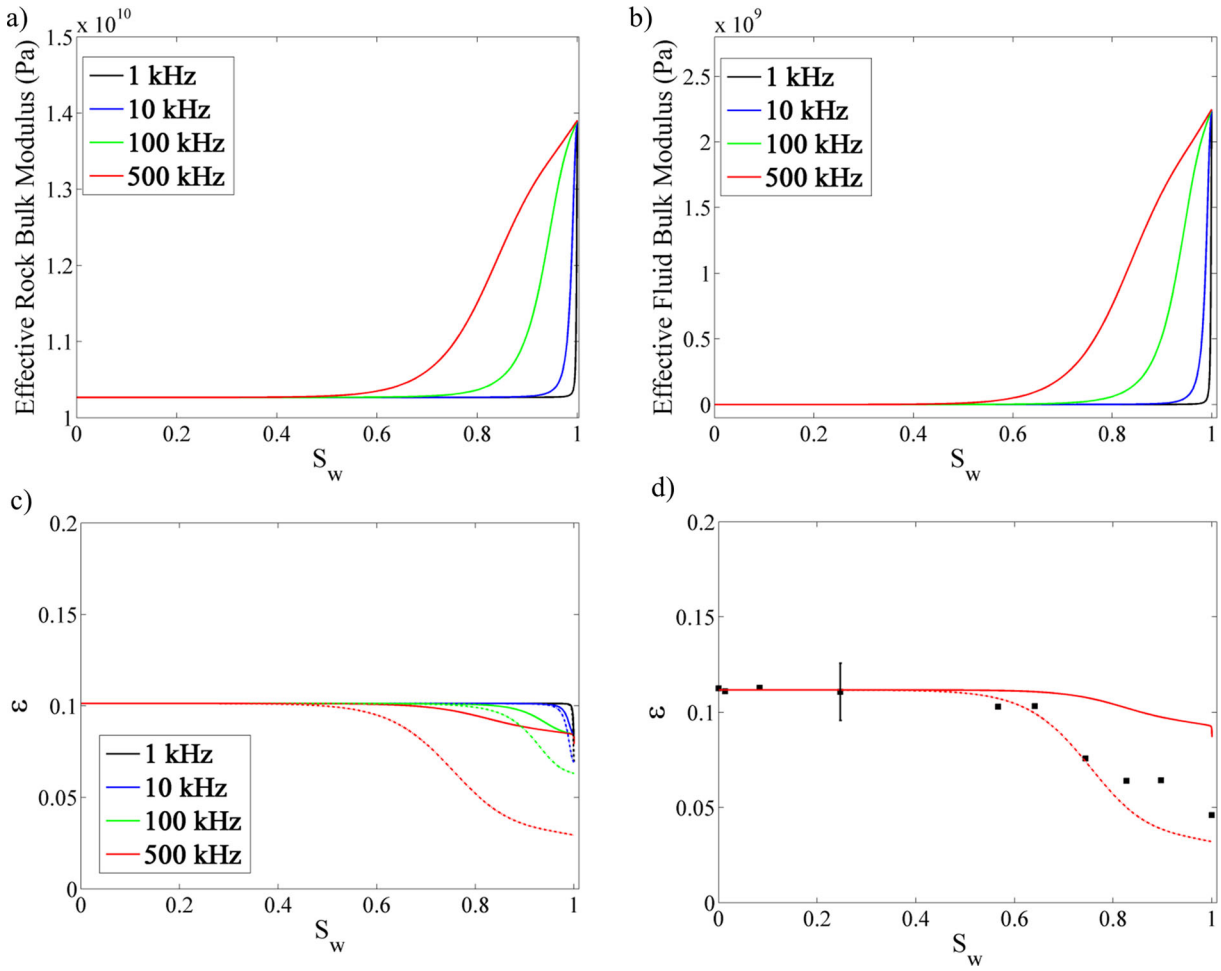

Figure 6. (a) White's model predictions of bulk modulus versus S_w at different frequencies (using a constant patch size of 0.5 mm). (b) Corresponding effective fluid bulk modulus calculated using Gassmann's equation. (c) *P*-wave anisotropy parameter 'ε' versus S_w without dispersion (solid lines) and with dispersion (dotted lines) from the fractured rock model, obtained after applying fracture corrections to the bulk moduli from Fig. 6(a). (d) Comparing the experimentally observed trend for 'ε' (black squares) to model predictions at 500 kHz without dispersion (solid line) and with dispersion (dotted line) from the fractured rock model.

and d). We see that at higher S_w values the maximum fluid effect is at 0° to the fracture normal while the minimum fluid effect is at 90° to the fracture normal with a greater fluid effect seen when dispersion is considered from the fracture rock model as well (Fig. 7d) compared to dispersion considered from White's model alone (Fig. 7c). Therefore, the fluid effect increases as *P*-wave propagation goes from parallel (90°) to perpendicular (0°) to the fracture normal. The critical S_w where the fluid effect begins depends on the critical S_w when the *P*-wave modulus goes from relaxed to unrelaxed behaviour, which comes in from the frequency dependent model of White (1975) in this modelling approach.

The presence of partial liquid–gas saturation and the presence of fractures are both known to cause dispersion in rocks, believed to be as a result of wave-induced fluid flow (see Müller *et al.* 2010). It can be seen that as the effective isotropic background rock property (in this case as a result of changing water saturation) changes, this has an effect on the anisotropy of the fractured rock, a result which may not be obvious. A similar observation was made in the numerical study (although dispersion was not considered) by Sil *et al.* (2011) where they showed that changes in the isotropic background properties as a result of changes in water saturation and porosity had an effect on *P*-wave anisotropy of the fractured rock considered. It then follows that if the effective isotropic background property is frequency dependent, then the effect on *P*-wave anisotropy would be frequency dependent. Dispersion as a result of wave-induced fluid flow is also known to be caused by the presence of fractures (Chapman *et al.* 2003; Gurevich *et al.* 2009; Kong *et al.* 2013). It can be seen that a larger fluid effect on anisotropy is observed when dispersion is considered as a result of wave-induced fluid flow from the fractured rock model (Fig. 6d).

For both 'ε' and the *P*-wave modulus, we see good agreement with our experimental data when we consider dispersion from both the changing background rock and the fractured rock. This observation suggests that not only could the effect of saturation on the bulk property of the rock have an effect on *P*-wave anisotropy, but the effect of the fluid on the compliance of the fractures could also be important and both effects can be frequency dependent. We realize that we have taken a simplistic (but yet intuitive) approach to modelling our data. However, partial liquid–gas saturation effects on seismic properties of rocks already constitute a complex problem and the presence of fractures complicates it further as the actual mechanisms in an experiment like this and their interactions would be very complex. Therefore, using this simple modelling approach we can gain some valuable insight into potential mechanisms causing the observed trend. Further advances in theoretical and experimental studies are needed to give a better understanding of the

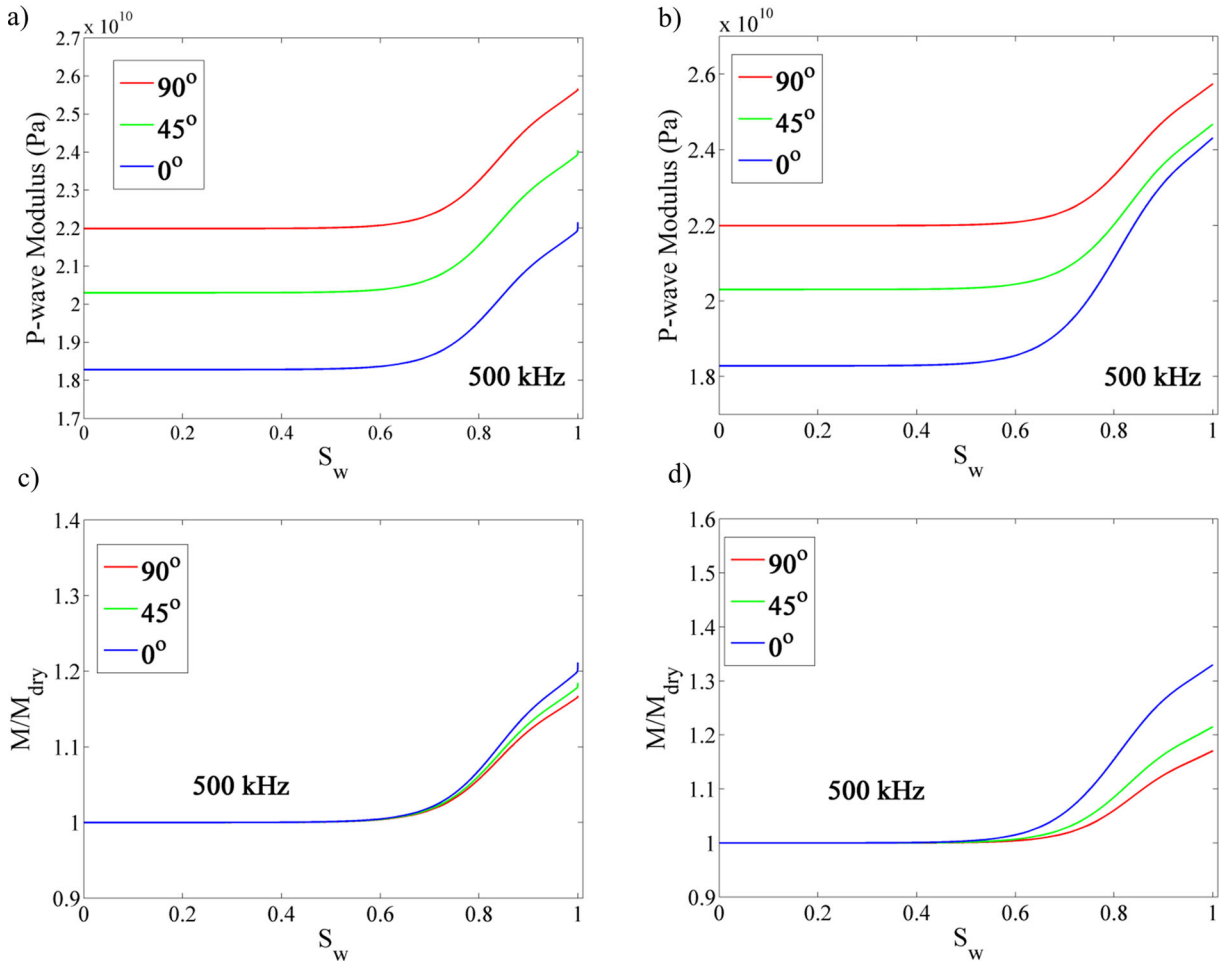

Figure 7. (a) Model predictions of *P*-wave moduli versus S_w at 500 kHz without dispersion from the fractured rock model. (b) Model predictions of *P*-wave moduli versus S_w at 500 kHz with dispersion included from the fractured rock model. (c) Model predictions of ratios of *P*-wave moduli to the dry *P*-wave modulus without dispersion from the fractured rock model. (d) Model predictions of ratios of *P*-wave moduli to the dry *P*-wave modulus with dispersion included from the fractured rock model.

mechanisms involved and to isolate the dominant mechanisms at different conditions.

Our results show that water saturation affects the *P*-wave anisotropy of fractured rocks and this effect could be frequency dependent due to wave induced fluid flow mechanisms. This effect could be important for seismic characterization of fractured reservoirs containing gas. The dispersion could be exploited for gas saturation estimates as dispersion has been shown to be sensitive to the amount of gas saturation (e.g. Wu *et al.* 2014). Understanding the effect of water saturation on *P*-wave anisotropy could help improve seismic characterization of fractured reservoirs. The different frequencies at which elastic wave data are acquired makes understanding the frequency-dependence of these effects important.

5 CONCLUSION

We have presented experimental observations of two-phase saturation (water–air) effects on *P*-wave anisotropy in synthetic fractured sandstone. The results show a significant effect of water saturation on *P*-wave anisotropy of the fractured rock. We observed the fluid effect is greatest perpendicular to the fractures and lowest parallel to the fractures. As a result, the *P*-wave anisotropy parameter 'ε' decreases as the effective modulus of the rock increases. The effective modulus of the rock is frequency-dependent due to wave-induced fluid flow mechanisms which act to stiffen the rock and the fractures. A larger effect is seen when dispersion due to wave-induced fluid flow is included from the fractured rock model. The frequency-dependence could be as a result of the presence of partial liquid/gas saturation or due to the presence of fractures or a combination of both. Our simple modelling approach shows good qualitative agreement with the experimental data. This frequency-dependent influence of water saturation on *P*-wave anisotropy could help improve fractured reservoir characterization.

ACKNOWLEDGEMENTS

The authors wish to thank the United Kingdom Natural Environment Research Council and the sponsors of the Edinburgh Anisotropy Project for supporting this work which forms part of the PhD studies of Kelvin Amalokwu under a NERC-BGS PhD studentship. We would also like to thank Jeremy Sothcott for helping with setting up the experiment.

REFERENCES

Amalokwu, K., Chapman, M., Best, A.I., Sothcott, J., Minshull, T.A. & Li, X.-Y., 2015. Experimental observation of water saturation effects on shear

wave splitting in synthetic rock with fractures aligned at oblique angles, *Geophys. J. Int.,* **200,** 17–24.
Bakulin, A., Grechka, V. & Tsvankin, I., 2000. Estimation of fracture parameters from reflection seismic data—Part I: HTI model due to a single fracture set, *Geophysics,* **65,** 1788–1802.
Best, A.I., 1992. The prediction of the reservoir properties of sedimentary rocks from seismic measurements, *PhD thesis,* University of Reading.
Bourbie, T. & Zinszner, B., 1985. Hydraulic and acoustic properties as a function of porosity in Fontainebleau Sandstone, *J. geophys. Res.: Solid Earth,* **90,** 11 524–11 532.
Brie, A., Pampuri, F., Marsala, A. & Meazza, O., 1995. Shear sonic interpretation in gas-bearing sands, in *Proceedings of the SPE Annual Technical Conference and Exhibition*, Dallas, Texas.
Cadoret, T., Marion, D. & Zinszner, B., 1995. Influence of frequency and fluid distribution on elastic wave velocities in partially saturated limestones, *J. geophys. Res.: Solid Earth,* **100,** 9789–9803.
Carcione, J., Helle, H. & Pham, N., 2003. White's model for wave propagation in partially saturated rocks: comparison with poroelastic numerical experiments, *Geophysics,* **68,** 1389–1398.
Carcione, J., Gurevich, B., Santos, J. & Picotti, S., 2013. Angular and frequency-dependent wave velocity and attenuation in fractured porous media, *Pure appl. Geophys.,* **170,** 1673–1683.
Chapman, M., 2003. Frequency-dependent anisotropy due to meso-scale fractures in the presence of equant porosity, *Geophys. Prospect.,* **51,** 369–379.
Chapman, M., Maultzsch, S., Liu, E. & Li, X.-Y., 2003. The effect of fluid saturation in an anisotropic multi-scale equant porosity model, *J. appl. Geophys.,* **54,** 191–202.
Dellinger, J. & Vernik, L., 1994. Do traveltimes in pulse-transmission experiments yield anisotropic group or phase velocities?, *Geophysics,* **59,** 1774–1779.
Gregory, A., 1976. Fluid saturation effects on dynamic elastic properties of sedimentary rocks, *Geophysics,* **41,** 895–921.
Gurevich, B., Brajanovski, M., Galvin, R.J., Müller, T.M. & Toms-Stewart, J., 2009. *P*-wave dispersion and attenuation in fractured and porous reservoirs—poroelasticity approach, *Geophys. Prospect.,* **57,** 225–237.
Hudson, J.A., 1981. Wave speeds and attenuation of elastic waves in material containing cracks, *Geophys. J. R. astr. Soc.,* **64,** 133–150.
King, M.S., Marsden, J.R. & Dennis, J.W., 2000. Biot dispersion for *P*- and *S*-wave velocities in partially and fully saturated sandstones, *Geophys. Prospect.,* **48,** 1075–1089.
Kong, L., Gurevich, B., Müller, T.M., Wang, Y. & Yang, H., 2013. Effect of fracture fill on seismic attenuation and dispersion in fractured porous rocks, *Geophys. J. Int.,* **195,** 1679–1688.
Li, X.Y., 1999. Fracture detection using azimuthal variation of *P*-wave moveout from orthogonal seismic survey lines, *Geophysics,* **64,** 1193–1201.
Lynn, H.B., Simon, K.M., Bates, C.R. & Dok, R.V., 1996. Azimuthal anisotropy in *P*-wave 3-D (multiazimuth) data, *Leading Edge,* **15,** 923–928.
Mavko, G. & Mukerji, T., 1998. Bounds on low-frequency seismic velocities in partially saturated rocks, *Geophysics,* **63,** 918–924.
Mavko, G. & Nolen-Hoeksema, R., 1994. Estimating seismic velocities at ultrasonic frequencies in partially saturated rocks, *Geophysics,* **59,** 252–258.
Mavko, G., Mukerji, T. & Dvorkin, J., 2009. *The Rock Physics Handbook,* Cambridge Univ. Press.
Müller, T., Gurevich, B. & Lebedev, M., 2010. Seismic wave attenuation and dispersion resulting from wave-induced flow in porous rocks—a review, *Geophysics,* **75,** 75A 147–75A 164.
Murphy, W.F., 1982. Effects of partial water saturation on attenuation in Massillon sandstone and Vycor porous glass, *J. acoust Soc. Am.,* **71,** 1458–1468.
Murphy, W.F., 1984. Acoustic measures of partial gas saturation in tight sandstones, *J. geophys. Res.: Solid Earth,* **89,** 11 549–11 559.
Rathore, J.S., Fjaer, E., Holt, R.M. & Renlie, L., 1995. *P*- and *S*-wave anisotropy of a synthetic sandstone with controlled crack geometry, *Geophys. Prospect.,* **43,** 711–728.
Rüger, A., 1997. *P*-wave reflection coefficients for transversely isotropic models with vertical and horizontal axis of symmetry, *Geophysics,* **62,** 713–722.
Rüger, A. & Tsvankin, I., 1997. Using AVO for fracture detection: analytic basis and practical solutions, *Leading Edge,* **16,** 1429–1434.
Sayers, C.M. & Rickett, J.E., 1997. Azimuthal variation in AVO response for fractured gas sands, *Geophys. Prospect.,* **45,** 165–182.
Sil, S., Sen, M. & Gurevich, B., 2011. Analysis of fluid substitution in a porous and fractured medium, *Geophysics,* **76,** WA157–WA166.
Thomsen, L., 1986. Weak elastic anisotropy, *Geophysics,* **51,** 1954–1966.
Thomsen, L., 1995. Elastic anisotropy due to aligned cracks in porous rock, *Geophys. Prospect.,* **43,** 805–829.
Tillotson, P., Chapman, M., Best, A.I., Sothcott, J., McCann, C., Shangxu, W. & Li, X.-Y., 2011. Observations of fluid-dependent shear-wave splitting in synthetic porous rocks with aligned penny-shaped fractures, *Geophys. Prospect.,* **59,** 111–119.
Tillotson, P., Chapman, M., Sothcott, J., Best, A.I. & Li, X.-Y., 2014. Pore fluid viscosity effects on *P*- and *S*-wave anisotropy in synthetic silica-cemented sandstone with aligned fractures, *Geophys. Prospect.,* **62,** 1238–1252.
White, J.E., 1975. Computed seismic speeds and attenuation in rocks with partial gas saturation, *Geophysics,* **40,** 224–232.
Winterstein, D.F., 1986. Anisotropy effects in *P*-wave and SH-wave stacking velocities contain information on lithology, *Geophysics,* **51,** 661–672.
Wu, X., Chapman, M., Li, X.-Y. & Boston, P., 2014. Quantitative gas saturation estimation by frequency-dependent amplitude-versus-offset analysis, *Geophys. Prospect.,* **62,** 1224–1237.
Yao, Q., Han, D.-h., Yan, F. & Zhao, L., 2013. Fluid substitution with dynamic fluid modulus: facing the challenges in heterogeneous rocks, in *Proceedings of the SEG Technical Program Expanded Abstracts 2013,* Houston, Texas, pp. 2851–2855.

SUPPORTING INFORMATION

Additional Supporting Information may be found in the online version of this paper:

Saturation method (http://gji.oxfordjournals.org/lookup/suppl/doi:10.1093/gji/ggv192/-/DC1).

Please note: Oxford University Press is not responsible for the content or functionality of any supporting materials supplied by the authors. Any queries (other than missing material) should be directed to the corresponding author for the paper.